Developmental Cell
Article

Mammary Morphogenesis and Regeneration Require the Inhibition of EMT at Terminal End Buds by Ovol2 Transcriptional Repressor

Kazuhide Watanabe,[1] Alvaro Villarreal-Ponce,[1] Peng Sun,[1] Michael L. Salmans,[1] Magid Fallahi,[1] Bogi Andersen,[1,2] and Xing Dai[1,*]
[1]Department of Biological Chemistry, School of Medicine, University of California, Irvine, Irvine, CA 92697, USA
[2]Department of Medicine, School of Medicine, University of California, Irvine, Irvine, CA 92697, USA
*Correspondence: xdai@uci.edu
http://dx.doi.org/10.1016/j.devcel.2014.03.006

SUMMARY

Epithelial cells possess remarkable plasticity, having the ability to become mesenchymal cells through alterations in adhesion and motility (epithelial-to-mesenchymal transition [EMT]). However, how epithelial plasticity is kept in check in epithelial cells during tissue development and regeneration remains to be fully understood. Here we show that restricting the EMT of mammary epithelial cells by transcription factor Ovol2 is required for proper morphogenesis and regeneration. Deletion of *Ovol2* blocks mammary ductal morphogenesis, depletes stem and progenitor cell reservoirs, and leads epithelial cells to undergo EMT in vivo to become nonepithelial cell types. Ovol2 directly represses myriad EMT inducers, and its absence switches response to TGF-β from growth arrest to EMT. Furthermore, forced expression of the repressor isoform of Ovol2 is able to reprogram metastatic breast cancer cells from a mesenchymal to an epithelial state. Our findings underscore the critical importance of exquisitely regulating epithelial plasticity in development and cancer.

INTRODUCTION

The induction of pluripotency in terminally differentiated cell types (Takahashi and Yamanaka, 2006) and the existence of pluripotent cells in physiological adult tissues (Roy et al., 2013) highlight the remarkable lineage plasticity of somatic cells. Although this plasticity offers immense opportunities for regenerative medicine, it raises questions as to how to properly restrict plasticity during the dynamic processes of tissue development and regeneration. Cells of epithelial lineages can undergo phenotypic changes to gain mesenchymal features through an epithelial-to-mesenchymal transition (EMT) program (Kalluri and Weinberg, 2009). Complete EMT occurs during mesoderm or neural crest formation to generate fully committed mesenchymal cell types (Thiery et al., 2009), whereas partial and reversible EMT occurs during morphogenesis of certain epithelial tissues such as mammary gland (MG) (Nakaya and Sheng, 2013). Although much has been learned about the molecular mechanisms that promote EMT during early development and in cancer cells, genetic pathways that regulate partial EMT during tissue morphogenesis to maintain epithelial lineages are poorly characterized.

MG undergoes dramatic tissue growth and remodeling during puberty and pregnancy, generating not only luminal epithelial cells but also a unique mesenchymal-like epithelial population, namely, basal/myoepithelial cells (Watson and Khaled, 2008). Thus, MG serves as an ideal system to study the genetic circuits that control epithelial lineage plasticity. At puberty, mammary epithelial stem/progenitor cells that reside in the terminal end buds (TEBs) undergo collective migration to drive ductal morphogenesis (Ewald et al., 2008). This process involves the acquisition of motility while preserving overall epithelial integrity. Moreover, a partial loss and reestablishment of epithelial adhesion and polarity occur at the TEBs (Ewald et al., 2008, 2012; Kouros-Mehr and Werb, 2006; Nanba et al., 2001). These findings imply that both epithelial plasticity-promoting and -restricting mechanisms might be important for the morphogenic potential of TEB stem/progenitor cells (Godde et al., 2010). Pregnancy induces dramatic expansion and regression of epithelial components as well as dynamic remodeling of the stromal environment (Watson and Khaled, 2008), creating yet another developmental window where epithelial lineage plasticity may have to be intricately regulated. The basal/myoepithelial population of adult MG contains the so-called multipotent mammary stem cells (MaSCs) that, upon transplantation, are capable of regenerating an entire epithelial network composed of both luminal and basal/myoepithelial lineages (Shackleton et al., 2006; Stingl et al., 2006). Adult stem cells with bipotential or unipotential have also been found in the mammary basal compartment via lineage tracing under physiological conditions (Rios et al., 2014; Van Keymeulen et al., 2011). Recent, largely in vitro, studies have implicated several EMT-inducing transcription factors (EMT-TFs), such as Snail, Slug, and Zeb1, as important factors that promote stemness in normal and malignant mammary epithelial cells (MECs) (Chaffer et al., 2013; Guo et al., 2012; Mani et al., 2008; Nassour et al., 2012). However, the in vivo mechanisms that restrict epithelial lineage plasticity to safeguard differentiation and how such mechanisms regulate stem cell function during MG morphogenesis and regeneration remain poorly understood.

Here we provide in vivo evidence for a previously unrecognized mechanism that protects epithelial identity during mammary tissue morphogenesis and regeneration, which involves Ovo-like 2 (Ovol2), a member of the Ovo family of zinc finger TFs that are known to regulate epithelial development in *Drosophila* epidermis as well as mammalian skin and testis (Dai et al., 1998; Li et al., 2005; Nair et al., 2006). Using conditional knockout and lineage-tracing approaches, we demonstrate that *Ovol2*-deficient mammary stem/progenitor cells are prone to undergo EMT and exhibit reduced morphogenic and regenerative capacity. Our genome-wide analyses identify myriad essential players in the EMT program as direct targets of Ovol2 transcriptional repression. Furthermore, we show that reducing either Zeb1 expression or transforming growth factor β (TGF-β) signaling, both well-known for EMT-promoting activity (Xu et al., 2009), partially rescues *Ovol2* loss-induced mammary defects. Thus, protection of epithelial identity is essential for epithelial tissue morphogenesis and regeneration.

RESULTS

Conditional Deletion of *Ovol2* Results in Impaired Postnatal MG Development

Well-known EMT-promoting transcription factors Snail and Slug both contain a Snail1/GFI (SNAG) domain essential for repression of target gene expression (Chiang and Ayyanathan, 2013). Interestingly, mammalian Ovol proteins also contain a SNAG domain, and their expression was decreased upon culture-induced EMT of primary MECs (Ehmann et al., 1984) (Figure S1A available online). *Ovol2/OVOL2* transcripts were detected in immortalized and primary MECs, but not in fibroblasts or stromal cells (Figures S1B and S1C). In vivo, nuclear Ovol2 was present in the developing MG, predominantly in ductal epithelial cells and TEB body cells, but also in a subset of the ductal basal and TEB cap cells (Figure 1A). Together, these findings reveal a tight correlation between *Ovol2* expression and an epithelial status.

To study Ovol2's role in epithelial morphogenesis, we generated skin/mammary-specific knockout (SSKO) mice of *Ovol2* using *K14-Cre*. *K14-Cre* directs highly efficient recombination in mammary epithelial lineages but not the surrounding stroma (Figures S1D and S1E; Movies S1 and S2). Although mammary rudiments in 3-week-old SSKO mice did not show any detectable differences from *Ovol2*-intact controls, pubertal MG development was nearly abolished in SSKO mice (Figure 1B). Impaired ductal elongation persisted throughout life (Figure S1F). At later stages of pubertal development (>7–8 weeks), dramatic fibrotic reactions surrounding the remaining ductal system and TEBs were frequently observed in SSKO MGs (Figures 1C and 1D). This said, the SSKO MG fat pad environment was able to support normal mammary morphogenesis when transplanted with β-galactosidase (β-gal)-labeled *Ovol2*-intact mammary fragments, whereas the endogenous, *Ovol2*-defient mammary trees remained rudimentary (Figure 1E). Upon pregnancy, SSKO MGs showed severely reduced but still detectable alveologenesis and milk production (Figures S1G and S1H). Collectively, these data demonstrate an epithelial-intrinsic requirement for *Ovol2* in postnatal mammary development and an indirect impact of its loss on the surrounding stroma.

Despite minimal pubertal morphogenesis, luminal and basal specification of MECs was able to occur in the remnant ducts of SSKO MGs (Figure S1I). However, fluorescence-activated cell sorting (FACS) analysis revealed an imbalance between MEC subpopulations, with an initial reduction of the $Lin^{-}CD24^{+}CD29^{lo}CD61^{hi}$ luminal progenitor population evident at 4 weeks, followed by an additional reduction in the $Lin^{-}CD24^{+}CD29^{hi}$ MaSC-enriched basal population by 8 weeks (Figure 1F). Consistent with normal estrogen receptor (ER) expression in *Ovol2*-deficient luminal cells (Figure S1I), the mRNA level of *Areg* (amphiregulin), an estrogen-responsive factor essential for ER-mediated ductal elongation (Ciarloni et al., 2007), and the phosphorylation status of its downstream mediator ERK, was not altered (Figures S1J and S1K).

MMTV-Wnt1 transgenic mice develop a mammary hyperbranching phenotype (Tsukamoto et al., 1988). In *MMTV-Wnt1* females, *Ovol2* deletion led to severely delayed ductal elongation and accumulation of surrounding stromal components, but precocious side branching still occurred (Figures S1L–S1N). Interestingly, the primary and secondary ducts grew along the longitudinal axis of the fat pad in control *MMTV-Wnt1* MGs, but they were random and nondirectional in *MMVT-Wnt1;*SSKO MGs (Figure 1G). In contrast, the hyperplastic MG phenotype, characterized by extensive side branching in *MMTV-Wnt1* males, was unaffected by *Ovol2* loss (Figure S1O). Together, these results reveal a specific requirement for *Ovol2* in female hormone-driven, coordinated, and directional ductal epithelial morphogenesis. These findings also support the notion that TEB-mediated ductal elongation/branching and Wnt-induced side branching are likely fueled by different progenitor cell populations (Watanabe et al., 2014) and are regulated by *Ovol2*-dependent and -independent mechanisms, respectively.

Ovol2-Deficient TEBs Exhibit EMT-like Behavior

Given the central role of TEB in driving directional ductal morphogenesis, we performed genome-wide gene expression analysis on TEBs isolated from SSKO and control littermates (Figure 2A). To identify primary changes, we analyzed TEBs from 24- to 25-day-old mice, when morphological differences between control and SSKO were still minimal (Figure 1B). Gene set enrichment analysis (GSEA) (Subramanian et al., 2005) revealed increased expression of gene sets associated with EMT, metallopeptidase activity, extracellular matrix (ECM) remodeling, ECM-related TGF-β targets, or focal adhesion (Figure 2A; Table S1). In contrast, a gene set enriched in mitotic cell cycle was significantly reduced in SSKO TEBs (Figure 2A; Table S1).

When isolated TEBs were cultured in 3D-Matrigel in the presence of epidermal growth factor (EGF) and fibroblast growth factor 2 (FGF-2) (Ewald et al., 2008; Fata et al., 2007), control TEBs underwent collective migration, where finger-like structures invaded into the surrounding Matrigel without leading cellular extensions (Ewald et al., 2008) (Figure 2B; Figure S2A). SSKO TEBs displayed a strikingly distinct outgrowth pattern, where individual cells disseminated into the gel (Figure 2B). Whole-mount staining of the TEB outgrowths revealed that although control cells were maintained in cohesive and polarized structures with uncovered keratin 8 $(K8)^{+}$ luminal cells at the tip as expected (Ewald et al., 2012), Ovol2-deficient $K14^{+}$ basal cells and

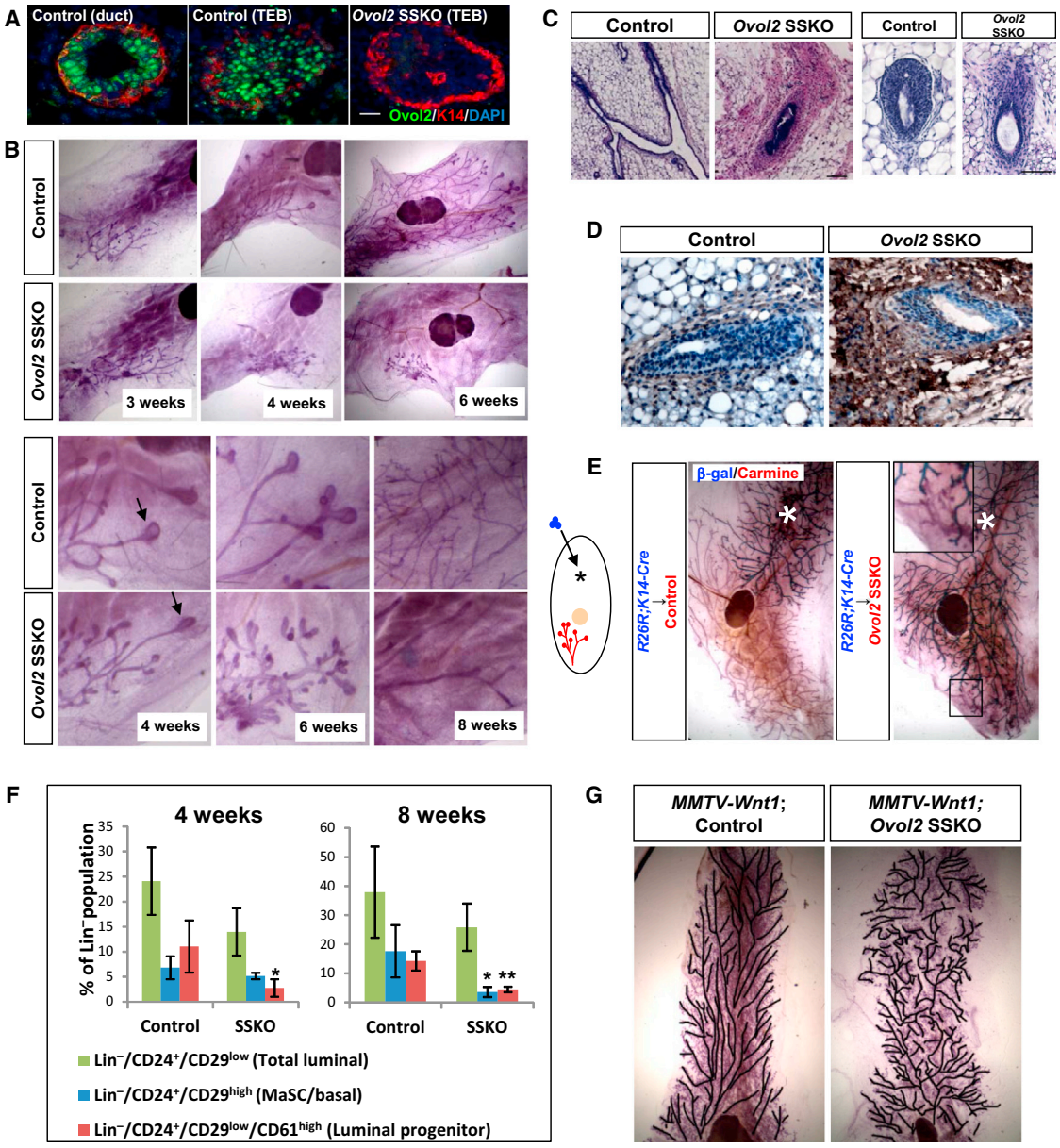

Figure 1. Loss of *Ovol2* Results in Severe Impairment of Mammary Ductal Morphogenesis

(A) Immunofluorescent staining of Ovol2 and K14 in developing MGs (4 weeks old) of the indicated genotypes.

(B) Whole-mount analysis of control and SSKO MGs during pubertal development. Whole glands (top) and TEB regions (bottom) are shown. Arrows indicate TEBs.

(C) Hematoxylin and eosin (H&E) images of ducts (right, 8 weeks old) and end bud regions (left, 7 weeks old). n > 5.

(D) Immunohistochemistry for fibronectin (8 weeks old). n > 5.

(E) Transplantation of β-gal$^+$ normal MECs (blue) into uncleared fat pads of control or SSKO hosts (n > 4 per genotype). Asterisks indicate the injection sites. Inset contains an enlarged image of the endogenous (red, β-gal$^-$), rudimentary tree generated by the SSKO host.

(F) FACS analysis of mammary populations from 4- and 8-week-old females of the indicated genotypes. Data indicate mean ± SD for the percentages of the indicated populations (n = 3–6). *p < 0.05, **p < 0.01.

(G) Primary/secondary ducts were outlined using Photoshop (Adobe) for whole-mount images from >20-week-old control and *Ovol2*-deficient *MMTV-Wnt1* MGs. Scale bars represent 50 μm (A and D); 100 μm (C).

See also Figure S1.

occasionally K8$^+$ luminal cells became depolarized and invasive (Figure 2C). Notably, fewer luminal cells were observed in the SSKO TEB outgrowths. *K14-Cre*-directed β-gal expression in TEB outgrowths derived from SSKO mice that also carried an *R26R* allele (*R26R;*SSKO) confirmed an epithelial origin of the invasive cells (Figure S2B). The invasive behavior of SSKO TEB cells was accompanied by a significant increase in the expression of EMT-related genes encoding structural factors such as

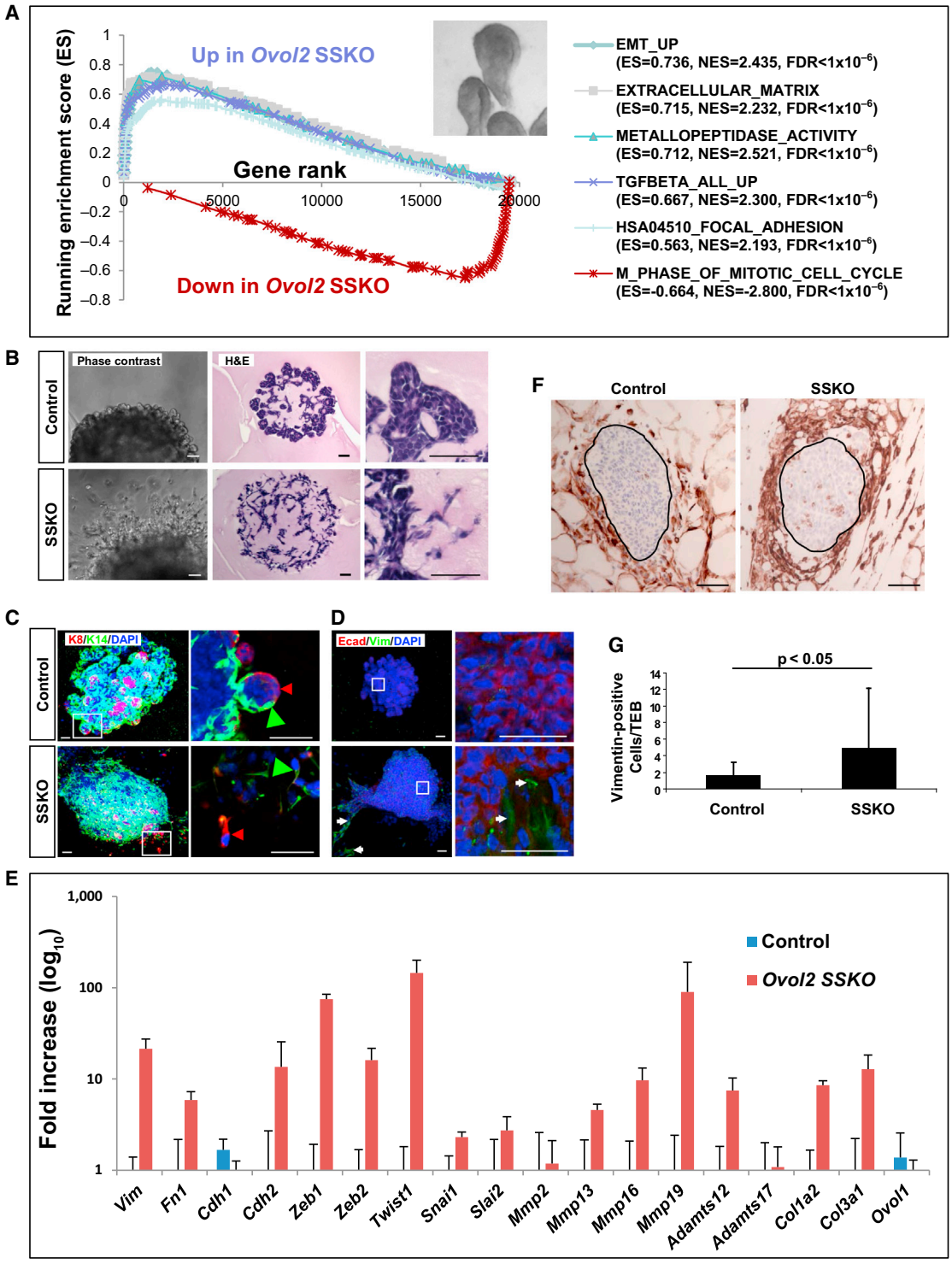

Figure 2. Molecular and Functional Characterizations of *Ovol2*-Deficient TEBs

(A) GSEA of microarray data on freshly isolated TEBs (inset) from control and SSKO mice (two biological replicates from a total of four to six mice per genotype). Gene lists used in GSEA were provided in Table S1. ES, enrichment score; NES, nominal enrichment score.

(B–D) Morphological and biochemical features of cultured TEBs. Images of phase-contrast and H&E-stained sections (B), whole-mount fluorescent staining for K8/K14 (C), and Vim/Ecad (D) are shown. All images were obtained from TEBs derived from 4-week-old mice and cultured for 5–8 days. In (C) and (D), enlarged images of the boxed areas are shown on the right. Red and green arrowheads in (C) point to $K8^+$ and $K14^+$ cells, respectively. Arrows in (D) point to Vim^+ cells.

(legend continued on next page)

Vim (vimentin [Vim]) and *Cdh2* (N-cadherin [Ncad]); EMT-TFs such as *Zeb1*, *Zeb2*, *Twist1*, *Snai1* (Snail), and *Snai2* (Slug); and ECM-remodeling factors such as *Mmp2*, *Mmp13*, *Mmp16*, *Mmp19*, *Adamts12*, *Adamts17*, *Col1a2*, and *Col3a1* (Figures 2D and 2E; Figure S2C). Upon transplantation into epithelia-cleared mammary fat pads of congenic host mice, SSKO TEBs generated abnormal structures with fibrosis-like stromal changes (Figure S2D).

Finally, we analyzed TEBs in situ. At 5 weeks, although most TEBs in control MGs were activated and proliferative, nearly half of the TEBs in SSKO MGs were quiescent (Figures S2E and S2F), which may have contributed to the reduction in luminal progenitor cells described above. $K6^+$ progenitor cells were also reduced in SSKO TEBs (Figure S2G). Because SSKO TEBs and MECs grew in vitro at a similar rate as controls (Figures S2H and S2I), the reduced proliferation is unlikely a primary effect of *Ovol2* deletion. Apoptotic cells were readily detectable in control but not SSKO TEBs (Figures S2J and S2K), suggesting reduced remodeling and lumen formation (Mailleux et al., 2008) in SSKO TEB. Importantly, abundant Vim^+ cells were observed in SSKO TEBs, whereas their presence in control TEBs was infrequent (Figures 2F and 2G). The number of Vim^+ cells in the stroma surrounding SSKO TEBs also appeared to be increased. Collectively, our data demonstrate that epithelial loss of *Ovol2* induces EMT-like molecular changes in the TEB microenvironment and impacts the cellular dynamics within the TEB.

MaSC/Basal Cells Transdifferentiate In Vitro and Undergo EMT In Vivo

Basal breast cancer cells are plastic and can readily switch to a cancer stem cell state (Chaffer et al., 2013). We reasoned that if normal MaSC/basal cells are also inherently plastic, then ablation of *Ovol2* may result in unchecked plasticity and loss of epithelial identity altogether. Indeed, although FACS-purified MaSC/basal cells from control mice formed solid colonies in Matrigel as described previously (Gu et al., 2013), some of the SSKO MaSC/basal cell-derived colonies became fibroblast-like and started muscle-like contraction (Figure 3A; Movies S3 and S4). This was accompanied by upregulated expression of known cardiac and skeletal muscle genes, namely, *Tnnt1*, *Tnnt2*, *Tnnt3*, and *Myl2* (Figure 3B), suggesting that in the absence of *Ovol2*, abnormal differentiation toward striated muscle lineages was activated in cultured MaSC/basal cells.

Next we tracked the fate of *Ovol2*-deficient MaSC/basal cells upon transplantation into cleared fat pads. Unlike the control MaSC/basal cells that efficiently produced well-branched mammary trees by 8 weeks after transplantation, MaSC/basal cells from *R26R;*SSKO mice were able to inoculate the fat pads but unable to form normal trees (Figure 3C). Two types of abnormal structures were observed in *R26R;*SSKO transplants: stunted-type structures consisted of short, rudimentary ducts that were histologically similar to the wild-type (WT) glands and EMT-type structures that were thin and contained epithelially derived (β-gal^+) fibroblast-like cells disseminating into the fat pads (Figure 3C). Both types were observed at a high frequency (seen in ~60% of the transplants) and sometimes coexisted in the same transplant (Figure 3C). EMT-type structures were also observed upon transplantation of *R26R;*SSKO mammary tissue fragments (Figure S3A). Limiting dilution transplantation revealed that the frequency of cells that generate such abnormal structures was approximately 1 in 2,000 in SSKO MaSC/basal cells, whereas the frequency of mammary repopulating cells in control counterparts was approximately 1 in 300 (Figure 3D). Together, these data provide strong evidence that *Ovol2*-deficient MaSC/basal cells or their progeny undergo EMT in vivo, and lose the ability to regenerate a normal mammary epithelial network.

To compare the ability of *Ovol2*-deficient and control MaSC/basal cells in contributing to mammary outgrowths within the same fat pad, and to distinguish between cell-autonomous and non-cell-autonomous effects, we next performed transplantation assays using a mixture of MaSC/basal cells from unlabeled WT and *R26R;*SSKO mice. Stunted- and EMT-type structures were frequently observed in β-gal^+ (thus *Ovol2*-deficient) outgrowths (11 and 10 of 17, respectively), but never in unlabeled WT outgrowths within the same fat pad (Figures S3B and S3C). As a control, in transplants derived from a mixture of unlabeled WT and *R26R;Ovol2*$^{flox/+}$*;K14-Cre* MaSC/basal cells, both β-gal^- and β-gal^+ cells produced morphologically normal outgrowths. At 2,000 cells/injection, β-gal^- and β-gal^+ trees were mostly well partitioned (Figure S3B), demonstrating clonal expansion (Welm et al., 2008). Only a single mosaic tree was observed, where the β-gal^+, *Ovol2*-deficient MaSC/basal cells were able to contribute to normal mammary tree production when WT cells were immediately adjacent. Transplantation of TEB organoids after adenoviral Cre (Ad-Cre) infection allowed more efficient generation of mosaic trees (Figures S3D and S3E). *R26R;Ovol2*$^{flox/+}$ and *R26R;Ovol2*$^{flox/-}$ organoids showed similar outgrowth take rates (~50%). However, although all outgrowths from *R26R;Ovol2*$^{flox/+}$ organoids contained mosaic trees, only 2 of 11 successful *R26R;Ovol2*$^{flox/-}$ transplants showed a mosaic pattern (Figure S3F). Taken together, these results demonstrate that *Ovol2*-deficient MaSC/basal cells produce primarily abnormal (stunted- or EMT-type) outgrowths and that even in the presence of *Ovol2*-intact MECs, *Ovol2*-deficient MECs rarely contribute to normal mammary tree formation.

To track the fate of *Ovol2*-deficient MECs in situ, we analyzed MGs from multiparious *R26R;*SSKO mice. Remarkably, whereas β-gal^+ cells existed only in the epithelial compartment of *R26R;Ovol2*$^{flox/+}$*;K14-Cre* control MGs, they were detected, albeit at low frequency, in the stroma of *R26R;*SSKO MGs, clustering within spindle-like structures that protruded from the otherwise normal-looking ducts (Figure 3E) and displaying an fibroblast-like morphology and Vim expression (Figure 3F). More than half of the multiparious *R26R;*SSKO MGs (14 of 24) contained abnormal structures with fibroblast-like cells, which were never

(E) RT-qPCR analysis of TEBs cultured for 8 days. Relative expression values (means ± SD; n = 4) are shown after normalization against a housekeeping gene *Gapdh*.

(F and G) Representative immunohistochemical images (F) and quantification (G) of Vim^+ cells at TEBs in vivo. A total of 20 TEBs from three mice per genotype were quantified for Vim^+ cells within the TEB body (G). Values represent mean ± SD. Scale bars represent 50 μm (B); 20 μm (C and D); 50 μm (F and G).
See also Figure S2 and Table S1.

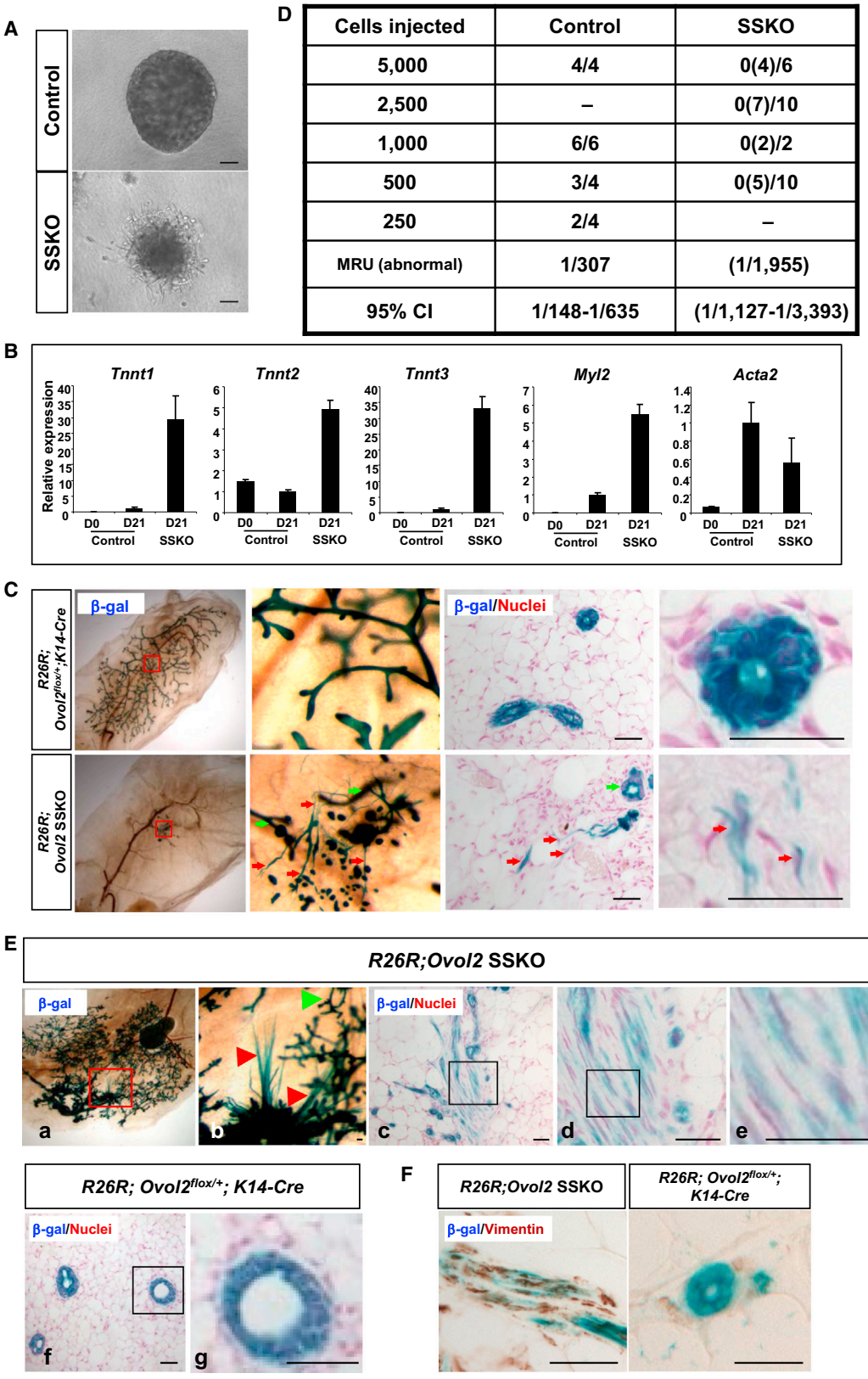

Figure 3. Ex Vivo and In Vivo Evidence That SSKO MaSC/Basal Cells Undergo EMT and Generate Nonepithelial Cell Types

(A) Morphology of MaSC/basal cell-derived colonies.

(B) RT-qPCR analysis of MaSC/basal cell cultures from (A). Relative expression values (mean ± SD; n = 2) are shown after normalization against *Gapdh*.

(legend continued on next page)

observed in control MGs. Collectively, our findings show unequivocally that without *Ovol2*, MECs are prone to undergo EMT-like changes and that actual EMT occurs when the MG undergoes extensive tissue remodeling such as after repeated pregnancy or upon transplantation.

Genome-wide Analysis Identifies Multiple EMT-Related Genes as Targets of Ovol2A Transcriptional Repression

To understand the molecular basis of *Ovol2* function, we performed genome-wide chromatin immunoprecipitation (ChIP) analysis of Ovol2 protein binding using high throughput sequencing (ChIP-seq). HC11, a normal mouse MEC line with stem/progenitor cell features (Williams et al., 2009), was used for the analysis. A total of 3,092 Ovol2-binding peaks, of which 1,328 were within 5% false discovery rate (FDR), were identified across the genome. The peaks were biased near transcriptional start sites (TSSs) of annotated genes, as more than 30% of them are located either within 1 kb upstream of the TSSs or 5′ untranslated regions (UTRs) (Figures 4A and 4B; Figures S4A and S4B). De novo motif-finding analysis identified a binding consensus CCGTTA (Figure 4C) that is identical to the in vitro Ovol1/2 binding sequence (Nair et al., 2007; Wells et al., 2009). The presence of this motif in a majority of the 5% FDR peaks (1,277 of 1,328) suggests that Ovol2 binds to the chromatin primarily through this sequence. GSEA of Ovol2-bound genes (within 2 kb from TSS; 770 genes) in the TEB microarray data set, wherein the genes were rank ordered for their differential expression between control and SSKO, revealed their significantly enriched expression ($p < 1 \times 10^{-6}$) in SSKO TEBs (Figure 4D), implying a repressor function of Ovol2 in vivo.

Genes that are both bound by Ovol2 (within 2 kb from TSSs) and upregulated in SSKO TEBs (signal-to-noise ratio > 0.75, top 841 genes in the microarray data) included those related to EMT, such as *Tgfb3*, *Vim*, *Zeb1*, *Zeb2*, and *Twist1* (Table S2). Genes related to cardiac differentiation or muscle function were also part of the direct target list. Moreover and consistent with previous studies (Li et al., 2005; Piloto and Schilling, 2010; Zhang et al., 2013), genes involved in neuronal differentiation, glycoprotein synthesis/intracellular trafficking, and transcriptional regulation were identified as direct Ovol2 targets. In addition to *Vim*, *Zeb1*, *Zeb2*, and *Twist1*, Ovol2 also bound to other EMT-TF genes such as *Snai1* and *Snai2*, as well as mesenchymal/neural-specific cadherin gene *Cdh2* (Figure S4B). *Vim* and *Zeb1* peaks were among the most prominent in the entire genome and notably, the Ovol2-binding peak in the first intron of *Zeb1* includes a known Myb/Ovol-binding consensus that was identified as a responsible site in the mouse *Twirler* mutation (Kurima et al., 2011).

To validate ChIP-seq findings, we established immortalized mouse mammary cell lines (iMMECs) from *Ovol2*$^{flox/-}$ MECs [iMMEC(N)] or *MMTV-Wnt1;Ovol2*$^{flox/flox}$ tumor cells [iMMEC(T)] that allowed acute deletion of *Ovol2* (Figure S5A). These iMMECs expressed the Ovol2A repressor isoform but not the Ovol2B activator isoform or Ovol2C dominant-negative isoform (Li et al., 2002), and the expression of Ovol2A protein/mRNA was nearly abolished after Ad-Cre infection (Figure 4E; Figure S5B). Ovol2 binding to the EMT-related target genes was confirmed in both iMMEC(N) and iMMEC(T) cells and, as expected, ChIP signals were abrogated when *Ovol2* was deleted (Figure 4F; data not shown).

RT-quantitative PCR (qPCR) analysis revealed an overall trend of upregulation of the EMT-related Ovol2 target genes in Cre-treated iMMECs (Figure 5A). Among them, *Vim*, *Zeb1*, and *Snai2* were significantly upregulated upon *Ovol2* loss in both iMMEC(N) and iMMEC(T). Interestingly, the expression of *Cdh1* (E-cadherin [Ecad]) was not affected. At a protein level, we detected dramatic upregulation of Vim, Zeb1, and Ncad upon *Ovol2* loss, whereas Ecad level remained the same (Figures 5B and 5C). Some *Ovol2*-deficient iMMECs simultaneously expressed Vim and Ecad proteins (Figure 5B), consistent with an intermediate cellular state. Despite the changes in gene expression, *Ovol2* deletion did not exert any detectable effect on the morphology, doubling time, migration, or EGF response of iMMECs (Figures S5A and S5C–S5E), implicating a need for additional signals to induce functional EMT in this in vitro system. Regardless, our molecular findings are consistent with Ovol2 transcriptional repression of genes that execute the EMT program.

To test the hypothesis that the SNAG-containing Ovol2A repressor isoform is primarily responsible for repressing EMT genes, we introduced Ovol2A, Ovol2B, or Ovol2C (Figure 5D) into Ovol2-deficient iMMECs. All isoforms were expressed at a comparable level and located predominantly in the nuclei (Figures 5E and 5F). Ovol2A significantly rescued the *Ovol2* loss-induced expression of EMT genes, whereas Ovol2B or Ovol2C caused further upregulation of *Vim* and *Zeb1* (Figure 5G; Figure S5F). Furthermore, an Ovol2A derivative, Ovol2A/G_2H_2, where the C_2H_2 zinc finger DNA-binding domain is mutated, behaved like Ovol2B or Ovol2C (Figure 5G). These data indicate that Ovol2A represses EMT genes in MECs, repression requires its DNA binding activity, and other Ovol2 isoforms could potentially mediate derepression. To validate Ovol2 isoform functions in vivo, FACS-purified MaSC/basal cells from 4-week-old SSKO MGs were infected with lentiviral vectors expressing Ovol2A, Ovol2B, Ovol2C, or Ovol2A/G_2H_2 along with an internal ribosome entry site-GFP cassette that enabled us to trace the infected cells. Upon transplantation, whereas control lentivirus-infected SSKO MaSC/basal cells generated only stunted- or EMT-type structures, three of four transplants from Ovol2A lentivirus-transduced SSKO cells developed well-branched mammary outgrowths

(C) Cleared fat pad transplantation of FACS-purified MaSC/basal cells (n > 8 per genotype). Representative X-gal-stained whole-mount (left, middle) and histological (right) images are shown.
(D) Limiting dilution transplantation of MaSC/basal cells from the indicated genotypes. X-gal staining was performed 8 weeks after transplantation, and only β-gal$^+$ structures were quantified. Results from two independent experiments were summarized. MRU, mammary repopulating unit.
(E) Whole-mount X-gal staining (a and b) and histological (d–g) images of MGs from multiparous females of the indicated genotypes. b, d, e, and g are enlarged images of boxed areas in a, c, d, and e, respectively. Red and green arrows/arrowheads in (C) and (Eb) indicate EMT- and stunted-type structures, respectively.
(F) X-gal/Vim double staining of multiparous *R26R;*SSKO MGs. Inset shows staining of a duct from control MG.
Scale bars represent 50 μm (A, C, E, and F).
See also Figure S3.

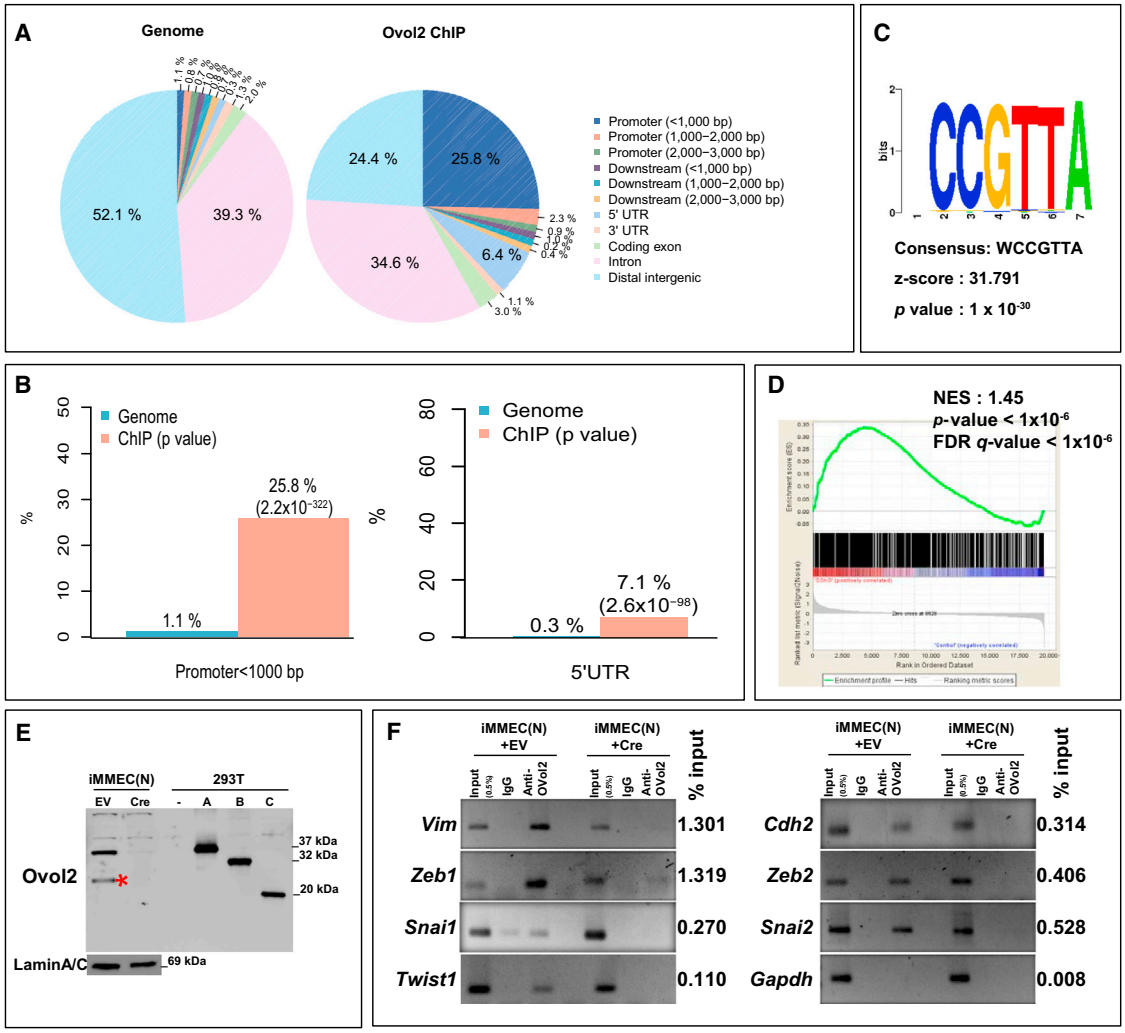

Figure 4. ChIP-Seq and ChIP-PCR Analyses Identify EMT Genes as Ovol2 Targets

(A) Distribution of Ovol2-binding regions on the genome relative to RefSeq genes. Intergenic region refers to all locations other than promoter, 5′ UTR, exon, intron, 3′ UTR, or downstream.

(B) Enrichment of Ovol2 binding at promoter (<1 kb) and 5′ UTR compared with random genomic distribution.

(C) Presence of Ovol-binding motif within the ChIP-seq peaks.

(D) GSEA performed on the TEB microarray data with Ovol2-bound gene set.

(E) Western blot analysis of Ovol2 with or without Cre induction in iMMEC(N). Lysates from 293T cells transiently expressing the indicated Ovol2 isoforms were run as size references. EV, empty vector. Asterisk indicates a previously unrecognized Ovol2 isoform the structure and function of which are currently unknown. LaminA/C was used as a loading control.

(F) ChIP-PCR. Note absence of ChIP signals in Ovol2-deficient iMMEC(N) cells. *Gapdh* promoter was used as a negative control. Values on the right of the gels represent percentage of input of Ovol2 occupancy obtained for iMMEC(N)+EV.

See also Figures S4 and S5 and Table S2.

(Figure 5H). In contrast, Ovol2B-, Ovol2C-, or Ovol2A/G_2H_2-transduced SSKO MaSC/basal cells did not generate any GFP^+ outgrowth (Figure 5H). These results demonstrate that Ovol2A is the major isoform that drives proper ductal morphogenesis.

Deregulation of Zeb1 and TGF-β Pathway Activities Contributes to *Ovol2* Loss-Induced Defect in Ductal Morphogenesis

To probe the functional relationship between deregulated EMT and impaired ductal morphogenesis, we asked whether depletion of *Zeb1*, which is the most tightly bound by Ovol2 in ChIP and among the most affected by *Ovol2* loss in TEBs and iMMECs, rescues the ductal morphogenesis defect in SSKO MGs. When infected with control small hairpin RNA (shRNA) (shScr)-expressing lentivirus (Figure S6A) followed by transplantation into cleared fat pads, SSKO MaSC/basal cells generated EMT-type structures (Figure 6A) identical to those described for *R26R;*SSKO transplants (Figure 3C). Remarkably, about half of the transplants derived from shZeb1-treated MaSC/basal cells generated well-branched outgrowths with a less mesenchymal appearance (Figures 6A and 6B). Thus, elevated *Zeb1* expression (and by inference, EMT) is at least in

part responsible for the ductal morphogenesis defect caused by loss of *Ovol2*.

The incomplete rescue of SSKO MG phenotype by *Zeb1* knockdown raises the possibility that additional molecular pathway(s) mediates the *Ovol2* loss-of-function effect. The negative effect of TGF-β on ductal elongation and branching has been extensively studied (Moses and Barcellos-Hoff, 2011). In keeping with *Tgfb3* being a potential Ovol2 target, we detected the upregulation of a subset of TGF-β-inducible genes (Figure 2A; Figure S6B) and remarkable activation of Smad2 (Figure 6C) in freshly isolated SSKO TEBs. We therefore asked whether inhibition of TGF-β signaling rescues the SSKO ductal morphogenesis defect. Treating 4–5-week-old mice with SB-431542, an inhibitor of TGF-β type I receptor kinase (Alk4/Alk5/Alk7) (Figure S6C), for 1 week resulted in a mild, but statistically significant rescue of ductal elongation and TEB maintenance in SSKO mice, whereas no significant effect was observed in controls (Figure 6D). Thus, elevated TGF-β signaling is in part mediating the SSKO MG phenotype.

To determine whether TGF-β signaling modifies the *Ovol2* loss-of-function phenotype by regulating EMT, we returned to TEB organoid culture. Because endogenous TGF-β signaling activity was not detectable under ex vivo culture condition (Figure 6C), administration of SB-431542 did not affect the dissemination of individual cells from cultured SSKO TEBs (Figure 6E), or their outgrowth and proliferation (Figures 6F–6H). Interestingly, however, addition of recombinant TGF-β exaggerated the fibroblast-like morphological conversion of SSKO TEB cells while suppressing the growth and branching of control TEBs (Figures 6E and 6F). These data demonstrate that although *Ovol2* loss-induced single cell dissemination does not require endogenous TGF-β signaling, loss of *Ovol2* alters TEB response to exogenous TGF-β from growth arrest to EMT.

Ovol2A, but Not Ovol2B or Ovol2C, Reprograms Highly Metastatic Breast Cancer Cells into an Epithelial State

EMT has been shown to trigger tumor cell motility and dissemination, thus promoting tumor invasion and metastasis (Valastyan and Weinberg, 2011). *Ovol2*'s role in suppressing EMT of normal MECs led us to examine a possible involvement of *OVOL2* in breast cancer. Using a publically available data set (Hoeflich et al., 2009), we found *OVOL2* and *OVOL1* to be highly expressed in breast cancer cells with low metastatic activity, in a manner that is similar to *CDH1* (Figure 7A). In contrast, the Ovol2-repressed EMT genes, including *ZEB1*, *ZEB2*, *SNAI1*, *SNAI2*, *TWIST1*, *VIM*, and *CDH2*, were highly expressed in metastatic breast cancer cell lines (Figure 7A). This correlation was confirmed at a protein level for select cell lines (Figure 7B). Moreover, *OVOL2* expression moderately correlated with epithelial gene expression at a genome scale (Figure S7A), and *OVOL2* was downregulated in the most aggressive, claudin-low-type and highly expressed in the luminal-type cancers (Di et al., 2013) (Figure S7B). Introduction of Ovol2A but not Ovol2B or Ovol2C to metastatic MDA-MB-231 cells induced Ecad and suppressed Vim and Zeb1 expression (Figures 7C and 7D) as well as inhibited their invasive activity (Figure 7E). We note that Ovol2A also exerted an antigrowth effect, because Ovol2A but Ovol2B or Ovol2C expression induced growth arrest slightly in MDA-MB-231 cells but more strongly in metastatic BT-549 cells (Figures 7F and 7G). In clinical samples, expression of *OVOL2* positively correlated with the overall and metastasis-free survival of postoperative breast cancer patients (Figure 7H). Collectively, these results implicate a suppressive role of Ovol2 in breast cancer invasion and metastasis, and they highlight the capability of the repressor isoform of Ovol2 in reprogramming metastatic breast cancer cells back to an epithelial state.

DISCUSSION

Our study identifies Ovol2 as a transcriptional gatekeeper of mammary epithelial differentiation. Ovol2 protects the epithelial identity of developing mammary progenitor cells by suppressing their tendency to undergo EMT during active morphogenesis. We demonstrate that epithelial progenitor cells can be reprogrammed in vivo into fibroblast-like cells by the loss of a single regulatory factor.

During pubertal ductal morphogenesis, TEB cells exhibit a unique collective-migration behavior that is suggested to represent a "morphogenetically active epithelial state" (Ewald et al., 2012). The correlation between compromised epithelial features and arrested ductal elongation in SSKO mice implicates a functional significance of collective cell migration in ductal morphogenesis. Our work thus underscores Ovol2 as a guardian of epithelial identity of a highly dynamic state. Specifically, we envision that Ovol2 prevents the TEB cells that have gained partial plasticity (Godde et al., 2010) from crossing the line to undergo complete EMT, thereby ensuring proper epithelial differentiation and morphogenesis.

Our data indicate that transcriptional suppression of EMT/mesenchymal genes by Ovol2, particularly the Ovol2A repressor isoform, is critical to maintain the identity of epithelial lineages. Interestingly, by virtue of its ability to bind the corresponding promoters, Ovol2 has the potential to repress nearly all major well-known EMT inducers, including *Zeb1*, *Zeb2*, *Twist1*, *Snai1*, and *Snai2*. As such, our work portraits Ovol2 as a critical molecular brake on EMT, and adds it to a short list of known EMT inhibitors, including Elf5, GATA3, GRHL2, Klf4, and the *miR200* family of microRNAs (Brabletz and Brabletz, 2010; Li et al., 2010; Chakrabarti et al., 2012; Cieply et al., 2012; Chou et al., 2013). The remarkable role of Ovol2A as a master EMT suppressor is further manifested by its ability to reprogram metastatic breast cancer cells back to an epithelial state, in keeping with a recent report demonstrating that Ovol factors can induce mesenchymal-to-epithelial transition (MET) in prostate and breast cancer cells (Roca et al., 2013).

The extent of Ovol2 repression of each individual EMT inducer may be jointly governed by the affinity of Ovol2 toward the promoter, and the variation in signaling milieus the cells are experiencing. Among all, *Zeb1* stands out as the most significant, based on its emergence as a top Ovol2 direct target, and the finding that depleting it alone partially rescues the *Ovol2* loss-of-function phenotype in vivo. It has been shown that resolution of bivalent chromatin domains at the *ZEB1* locus to an active state underlies the ability of basal human breast cancer cells to generate stem-like subpopulations (Chaffer et al., 2013). Moreover, *Zeb1* is the subject of intense cross-regulation with microRNAs for cancer cell stemness and EMT (Brabletz and Brabletz, 2010; Chaffer et al., 2013). Our work now reveals the importance

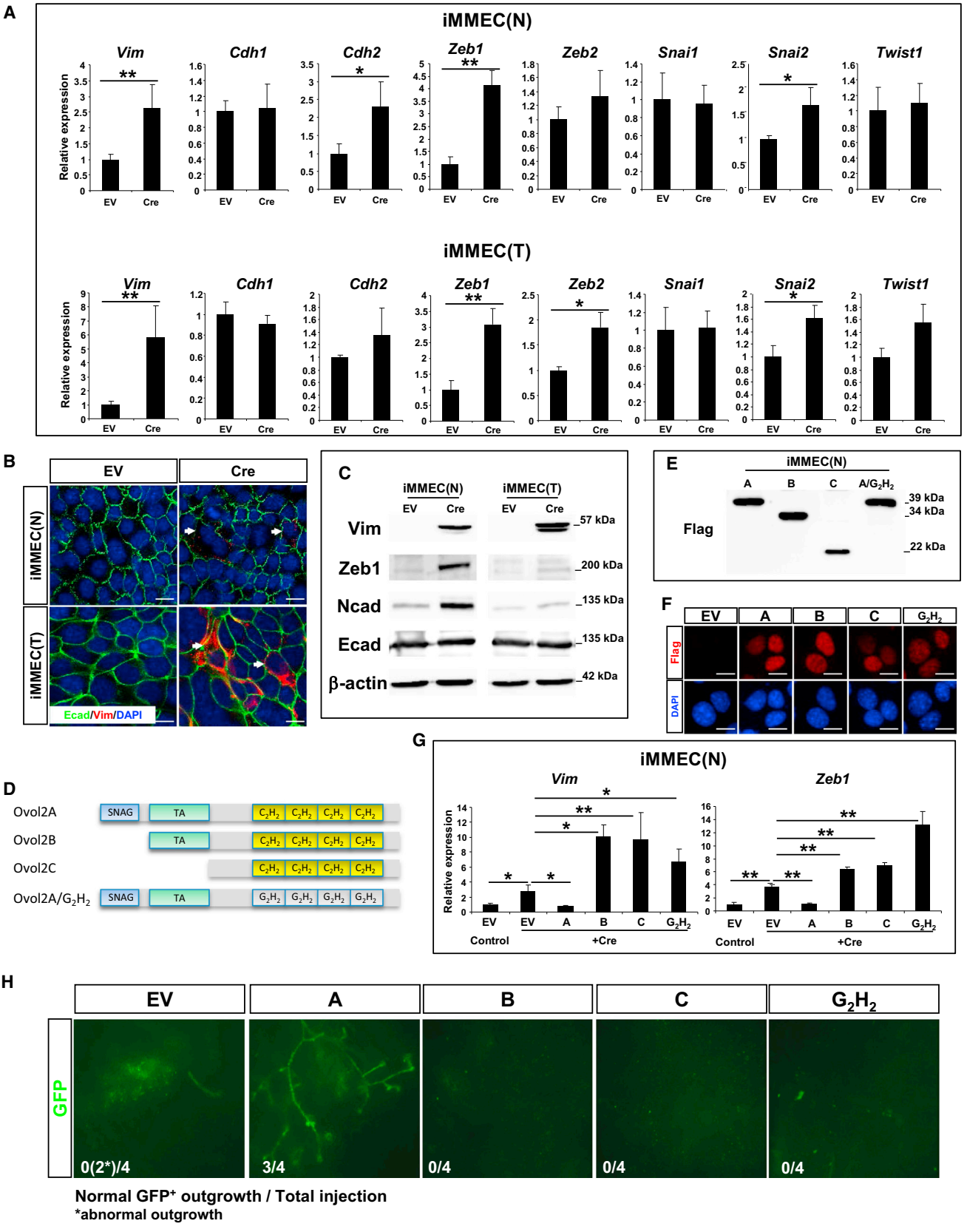

Normal GFP⁺ outgrowth / Total injection
***abnormal outgrowth**

(legend on next page)

of repressing *Zeb1* at the transcriptional level to preserve the capacity of MaSC/basal cells to regenerate a morphologically normal mammary epithelial tree. Thus, multilevel regulation of *Zeb1* lies at the center of achieving a delicate balance between epithelial plasticity and differentiation.

Interestingly, *Ovol2* deficiency-induced EMT-like changes are limited to aberrant gene expression in virgin MGs, but they become full-blown upon ex vivo culture, transplantation, or repeated pregnancies. This suggests that, in addition to a cell-intrinsic protection mechanism that involves Ovol2, environmental cues that ensure epithelial identity are also present in the virgin MG; complete EMT-like events such as single cell dissemination and conversion to fibroblast-like cell types only occur when the tissue environment is permanently or transiently disrupted. That mammary tissue environment exerts a strong influence on epithelial cells has been well documented, exemplified by the findings that MECs behave differently depending on the ECM microenvironment (Nguyen-Ngoc et al., 2012). In this context, the robust activation of TGF-β signaling, well-known for its ability to induce EMT (Xu et al., 2009) and remodel local environment (Moses and Barcellos-Hoff, 2011), in SSKO TEBs is particularly interesting. In TEB culture, *Ovol2* deletion induces the EMT phenotype independently of TGF-β signaling, likely through direct derepression of Zeb1 and other factors. In vivo, *Ovol2* loss induces the abnormal activation of TGF-β signaling that may have led to the growth cessation of TEBs, the ultimate loss of epithelial identity, and even stromal alterations. As such, the remarkable phenotype of SSKO MGs may represent a combined effect of epithelial-intrinsic machinery and epithelial-stromal interactions involving two major players, Zeb1 and TGF-β signaling.

Although loss of *Ovol2* alone is sufficient to induce a strong EMT phenotype in MaSC/basal MECs, simultaneous deletion of *Ovol1* and *Ovol2* is needed to induce aberrant epithelial plasticity in epidermal keratinocytes (see Lee et al., 2014 in this issue of *Developmental Cell*). It is tempting to speculate that the difference in EMT competence between MaSC/basal MECs and keratinocytes may root from the fact that the former gives rise to myoepithelial cells, a unique type of epithelial cell that possess partial mesenchymal features such as contractility and expression of mesenchymal genes. Thus, greater epithelial plasticity is likely tolerated and even desirable in mammary epithelia compared to skin epithelia, resulting in a somewhat looser protective mechanism for mammary epithelial identity. Furthermore, the differential response of TEB versus ductal cells to Ovol2 loss may be due to their different sensitivity to Ovol dosage. TEB cells might be more vulnerable than ductal cells because dynamic cell state transitions (EMT/MET) are required at the TEBs to support ductal morphogenesis.

Complete loss of epithelial identity could potentially unleash the ability of committed MaSC/basal cells to adopt different lineage fates and lose epithelial stemness. In this context, the gene expression and "beating" behavior of SSKO MaSC/basal cells upon long-term culturing are suggestive of aberrant differentiation toward striated muscle lineages, but future experiments are needed to determine whether this occurs in vivo. The ultimate reduction of the MaSC/basal subpopulation in addition to the luminal progenitor subpopulation in SSKO MGs as well as the compromised regenerating potential of SSKO MaSC/basal cells would be consistent with reduced stemness. Our study now offers tantalizing leads to future studies about definitive Ovol involvement in breast tissue and cancer stem cells, as well as in tumor metastasis.

EXPERIMENTAL PROCEDURES

Mouse Strains

Generation and genotyping of null and floxed *Ovol2* alleles were as described previously (Unezaki et al., 2007). *MMTV-Wnt1*, *mT/mG*, and *R26R* mice were purchased from The Jackson Laboratory [FVB/NJ-Tg(Wnt1)1Hev/J, B6.129(Cg)-Gt(ROSA)26Sortm4(ACTB-tdTomato,-EGFP)Luo/J, and B6.129S4-Gt(ROSA)26Sor^{tm1Sor}/J]. *R26R;*SSKO mice were generated in congenic C57BL/6 (B6) background by crossing *R26R;Ovol2*$^{+/-}$*;K14-Cre* males with *Ovol2*$^{flox/flox}$ females. *MMTV-Wnt1;*SSKO mice were generated in a B6:FVB/N-mixed background. All experiments have been approved by and conform to the regulatory guidelines of the International Animal Care and Use Committee of the University of California, Irvine (UCI).

Mammary Cell Preparation, FACS, and 3D-Matrigel Culture

Mammary cell preparation and FACS were performed as described previously (Gu et al., 2009, 2013). In brief, MGs were dissected from 4- to 5-week-old virgin females and dissociated by incubating for 16 hr with Gentle Collagenase/Hyaluronidase (STEMCELL Technologies). After vortexing and lysis of the red blood cells in NH_4Cl, a single-cell suspension was obtained by sequential dissociation of the fragments by gentle pipetting for 2 min in 0.25% trypsin (Sigma-Aldrich) and then for 2 min in 5 mg/ml dispase II (STEMCELL) plus 0.1 mg/ml DNase I (Sigma-Aldrich), followed by filtration through a 40 μm mesh. For all mammary cell isolations, viable cells were counted on a hemacytometer using trypan blue exclusion. Cell-surface marker staining was performed using the following antibodies and reagents: allophycocyanin (APC)-labeled CD31 (Becton Dickinson), APC-labeled CD45 (BD), APC-labeled TER119 (BD), phycoerythrin (PE)/Cy7-labeled CD24-PE/Cy7 (BD), fluorescein isothiocyanate (FITC) or PE-labeled CD29-FITC (BioLegend), and PE-labeled CD61 (BioLegend). Live-cell sorting was performed on an FACSAria cell sorter (BD) equipped with FACS DiVa6.0 software operating at low pressure (20 psi) using a 100 μm nozzle. Cell clusters and doublets were electronically gated out. Cells were routinely double sorted, and postsort analysis typically indicated purities of >90% with minimal cell death (<10%).

Primary MECs were cultured at a high density in MEC growth medium [Dulbecco's modified Eagle's medium (DMEM)/F12 (1:1) (Invitrogen) supplemented with 10% fetal bovine serum (FBS), 20 ng/ml EGF (Millipore), 5 μg/ml insulin (Sigma-Aldrich), and 1 μg/ml hydrocortisone (Sigma-Aldrich)].

Figure 5. Ovol2A Represses EMT Genes and Regulates Ductal Morphogenesis

(A) RT-qPCR analysis of the indicated EMT genes in iMMEC(N) and iMMEC(T) cells (values represent mean ± SD; n = 4).

(B) Immunofluorescent staining for Ecad and Vim. Arrows indicate Ecad/Vim double-positive cells.

(C) Western blot analysis of the indicated proteins in iMMEC(N) and iMMEC(T) cells. β−actin was used as a loading control.

(D) Diagram showing Ovol2 isoforms and mutant.

(E and F) Western blot analysis (E) and immunofluorescence (F) of iMMEC(N) infected with the indicated Ovol2 isoform/mutant-expressing lentiviruses.

(G) RT-qPCR analysis of *Vim* and *Zeb1* in iMMEC(N) cells that express the indicated Ovol2 isoforms/mutant (values represent mean ± SD; n = 4).

(H) Cleared fat pad transplant of SSKO MaSC/basal cells infected with the indicated Ovol2 isoform/mutant-expressing lentiviruses. Only well-branched outgrowths with GFP signals were counted. The number of abnormal GFP$^+$ structures (stunted or EMT type) is shown in parentheses. Scale bars represent 10 μm (B and F).

See also Figure S5.

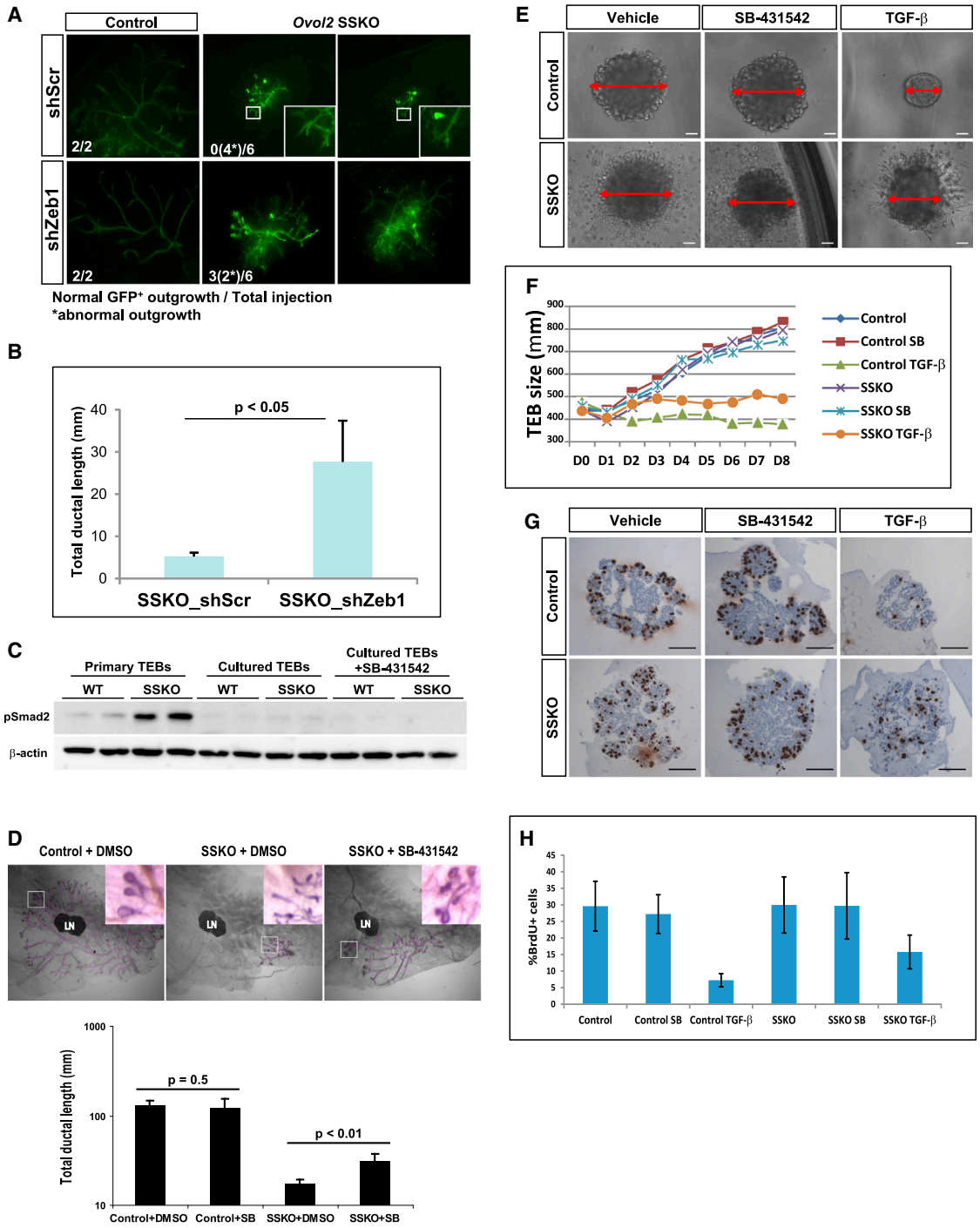

Figure 6. Involvement of Zeb1 and TGF-β Signaling in *Ovol2* Loss-Induced EMT and Ductal Morphogenesis Defect

(A) Cleared fat pad transplant of control or SSKO MaSC/basal cells infected with the indicated shRNA-expressing lentiviruses. Only well-branched outgrowths with GFP signals were counted. The number of abnormal GFP$^+$ structures (stunted or EMT type) is shown in parentheses.

(B) Quantification of ductal length (values represent mean ± SD; n = 6).

(C) Western blot analysis of Smad2 phosphorylation in freshly isolated (primary) and cultured (day 5) TEBs with and without SB-431542 (10 μM).

(D) Control and SSKO mice were intraperitoneally injected with vehicle (DMSO) or SB-431542 ([SB]10 mg/kg) at the age of 28, 30, 32, and 34 days, and MGs were analyzed at the age of 35 days (n = 6, 4, 6, and 8 for Control+DMSO, Control+SB, SSKO+DMSO, and SSKO+SB, respectively). Enlarged images of boxed areas in (A) and (C) are shown as insets.

(E–H) Morphology (day 8, E), growth (F), and bromodeoxyuridine (BrdU) staining (day 3, G and H) of control and SSKO TEBs cultured in the presence of SB-431542 (10 μM) or TGF-β (200 pM) (n > 10 per treatment). Values represent mean ± SD. Scale bars, 50 μm (E and G).

See also Figure S6.

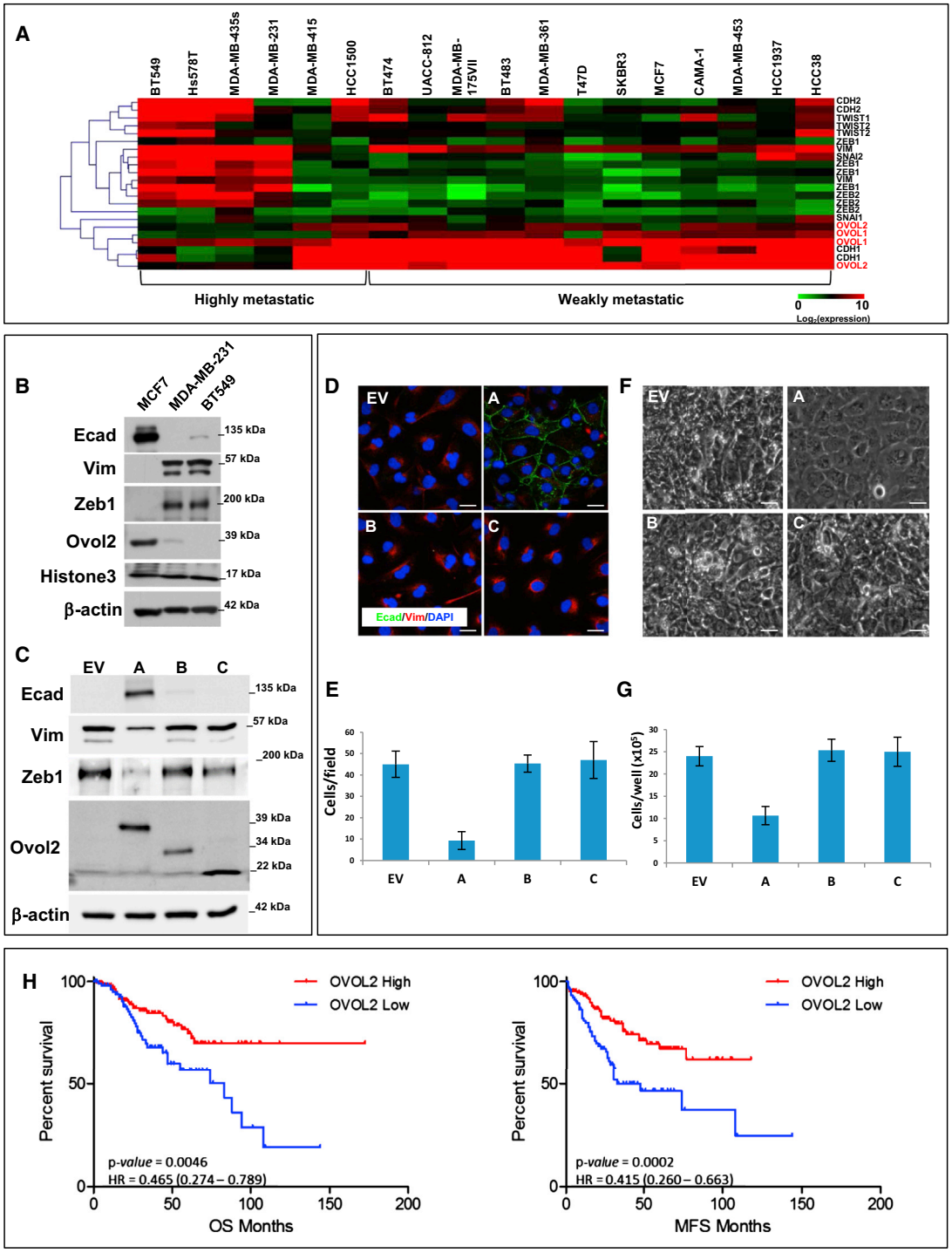

Figure 7. OVOL2/Ovol2 Expression and Function in Human Breast Cancer

(A) Heatmap for the expression of the indicated genes in various human breast cancer cell lines. A publically available data set (Gene Expression Omnibus GSE12790) (Hoeflich et al., 2009) was used for the analysis.

(B) Western blot analysis of the indicated proteins in select breast cancer cell lines.

(C–E) Effects of forced expression of Ovol2 isoforms on MDA-MB-231 cells. Western blotting (C), immunofluorescence (D), and Matrigel invasion assay (E; values represent mean ± SD, n = 3) were performed 4–5 days after lentiviral induction of the indicated Ovol2 isoforms.

(F and G) Growth inhibition of BT-549 cells by Ovol2A. Representative images (F) and quantification of cell number (mean ± SD, n = 3) after 5 days of plating (G) are shown.

(legend continued on next page)

Culture-induced EMT was observed after frequent passages (every 2 days) and seeding at a low density (<50%) (Figure S1A).

For 3D-Matrigel culture of MECs, single cells of sorted MaSC/basal population were gently resuspended in 100% chilled growth factor-reduced Matrigel (BD) and plated onto eight-well chamber slides at 2 × 10^4 cells/50 μl Matrigel/well. After set, the gel was covered with 400 μl of EpiCult-B medium (STEMCELL) containing 10 ng/ml EGF, 10 ng/ml FGF-2 (PeproTech), and 4 μg/ml heparin; the medium was replaced every 3 days. Cells were cultured for up to 21 days. RNA was isolated after disassociation of the Matrigel with dispase.

Transplantation Assays

For transplantation into uncleared fat pad, MG fragments (1–2 mm) from 8- to 10-week-old *R26R;K14-Cre* mice were injected into the distal side of #4 glands of 4-week-old control or SSKO syngeneic hosts (C57BL/6 or B6) (Figure 1D). The transplants were analyzed by X-gal/carmine double staining 8 weeks afterward. For cleared fat pad transplantation, FACS-sorted MaSC/basal cells (cell numbers are described in the text or legends for each transplantation), isolated TEBs or MG fragments (1–2 mm) were injected or inserted into the cleared fat pad of #4 glands of 3-week-old WT B6 hosts. Lentiviral infection before transplantation was performed as described previously (Gu et al., 2013). Outgrowths were analyzed 8 weeks after transplantation. GFP fluorescence was visualized with an MZFLIII fluorescent dissecting scope (Leica Microsystems) or E600 fluorescent microscope (Nikon). Statistical analysis of the take rate was as described previously (Gu et al., 2013).

TEB Isolation and Culture

TEB isolation was performed as described previously (Morris et al., 2004), with some modifications. MGs (#3–#5) were surgically isolated form adjacent tissues, minced into 1–2 mm pieces, and digested for 1 hr at 37°C in DMEM/F12 containing 5% FBS, 300 U/ml collagenase (Sigma-Aldrich), and 100 U/ml hyaluronidase (Sigma-Aldrich) with continuous shaking at 200 rpm and thorough mixing every 15 min. After lysis of the red blood cells in NH_4Cl, pellets were treated with 0.1 mg/ml DNase I (Sigma-Aldrich) for 10 min at 37°C. Pellets were then resuspended in DMEM/F12, and single TEBs were manually picked up under a dissection microscope with a fine micropipette (Figure 2A, inset). Microarray data from isolated TEBs are publically available (Gene Expression Omnibus GSE53923).

For 3D-Matrigel culture of TEBs, isolated TEBs were resuspended in growth factor-reduced Matrigel and plated onto eight-well chamber slides or ultralow attachment 96-well plates (Thermo Fisher Scientific) (three to five/well) under identical conditions as used for the MEC-3D culture mentioned above. Whole-mount staining was performed as described previously (Ewald et al., 2008). RNA was isolated at 8 days after disassociation of the Matrigel with dispase.

ChIP-Seq Analysis

ChIP was performed according to the previously described protocol (Gu et al., 2013), with some modifications. Sequencing was performed at UCI Genomics High Throughput Facility (GHTF) on a Genome Analyzer IIx (Illumina), one lane per sample, 36-bp singleton sequencing. ChIP-seq data are publically available (Gene Expression Omnibus GSE53925).

Additional details for the above-mentioned procedures, as well as procedures for cell culture, morphological and histological analysis of MGs, gene expression analysis, adeno- and lentiviral constructs, western blot analysis, and clinical data analysis are described in Supplemental Experimental Procedures.

SUPPLEMENTAL INFORMATION

Supplemental Information includes Supplemental Experimental Procedures, seven figures, two tables, and four movies and can be found with this article online at http://dx.doi.org/10.1016/j.devcel.2014.03.006.

ACKNOWLEDGMENTS

We thank the UCI GHTF and the Sue and Bill Gross Stem Cell Research Center Core Facility for expert service, Wen-Hwa Lee and Robert Edwards for advice and support. This work was supported by NIH grants R01-GM083089 and R01-AR47320 and Susan G. Komen grant KG110897 (to X.D.), the Irving Weinstein Foundation and R01-AR44882 (to B.A.). K.W. was supported by U.S. DOD BCRP postdoctoral fellowship W81XWH-10-1-0383. A.V.-P. and M.L.S. were supported by the California Institute of Regenerative Medicine Training Grant II Program.

Received: October 27, 2013
Revised: January 17, 2014
Accepted: March 12, 2014
Published: April 14, 2014

REFERENCES

Brabletz, S., and Brabletz, T. (2010). The ZEB/miR-200 feedback loop—a motor of cellular plasticity in development and cancer? EMBO Rep. *11*, 670–677.

Chaffer, C.L., Marjanovic, N.D., Lee, T., Bell, G., Kleer, C.G., Reinhardt, F., D'Alessio, A.C., Young, R.A., and Weinberg, R.A. (2013). Poised chromatin at the ZEB1 promoter enables breast cancer cell plasticity and enhances tumorigenicity. Cell *154*, 61–74.

Chakrabarti, R., Hwang, J., Andres Blanco, M., Wei, Y., Lukačišin, M., Romano, R.A., Smalley, K., Liu, S., Yang, Q., Ibrahim, T., et al. (2012). Elf5 inhibits the epithelial-mesenchymal transition in mammary gland development and breast cancer metastasis by transcriptionally repressing Snail2. Nat. Cell Biol. *14*, 1212–1222.

Chiang, C., and Ayyanathan, K. (2013). Snail/Gfi-1 (SNAG) family zinc finger proteins in transcription regulation, chromatin dynamics, cell signaling, development, and disease. Cytokine Growth Factor Rev. *24*, 123–131.

Chou, J., Lin, J.H., Brenot, A., Kim, J.W., Provot, S., and Werb, Z. (2013). GATA3 suppresses metastasis and modulates the tumour microenvironment by regulating microRNA-29b expression. Nat. Cell Biol. *15*, 201–213.

Ciarloni, L., Mallepell, S., and Brisken, C. (2007). Amphiregulin is an essential mediator of estrogen receptor alpha function in mammary gland development. Proc. Natl. Acad. Sci. USA *104*, 5455–5460.

Cieply, B., Riley, P., 4th, Pifer, P.M., Widmeyer, J., Addison, J.B., Ivanov, A.V., Denvir, J., and Frisch, S.M. (2012). Suppression of the epithelial-mesenchymal transition by Grainyhead-like-2. Cancer Res. *72*, 2440–2453.

Dai, X., Schonbaum, C., Degenstein, L., Bai, W., Mahowald, A., and Fuchs, E. (1998). The ovo gene required for cuticle formation and oogenesis in flies is involved in hair formation and spermatogenesis in mice. Genes Dev. *12*, 3452–3463.

Di, L.J., Byun, J.S., Wong, M.M., Wakano, C., Taylor, T., Bilke, S., Baek, S., Hunter, K., Yang, H., Lee, M., et al. (2013). Genome-wide profiles of CtBP link metabolism with genome stability and epithelial reprogramming in breast cancer. Nat. Commun. *4*, 1449.

Ehmann, U.K., Peterson, W.D., Jr., and Misfeldt, D.S. (1984). To grow mouse mammary epithelial cells in culture. J. Cell Biol. *98*, 1026–1032.

Ewald, A.J., Brenot, A., Duong, M., Chan, B.S., and Werb, Z. (2008). Collective epithelial migration and cell rearrangements drive mammary branching morphogenesis. Dev. Cell *14*, 570–581.

Ewald, A.J., Huebner, R.J., Palsdottir, H., Lee, J.K., Perez, M.J., Jorgens, D.M., Tauscher, A.N., Cheung, K.J., Werb, Z., and Auer, M. (2012). Mammary collective cell migration involves transient loss of epithelial

(H) Kaplan-Meier curves for overall survival (OS) or metastasis-free survival (MFS) of breast cancer patients with high (red) or low (blue) *OVOL2* expression. A total of 255 samples in the UNC337 data set had breast cancer patient survival data and were used for the analysis.
Scale bars, 20 μm (D and F).
See also Figure S7.

features and individual cell migration within the epithelium. J. Cell Sci. *125*, 2638–2654.

Fata, J.E., Mori, H., Ewald, A.J., Zhang, H., Yao, E., Werb, Z., and Bissell, M.J. (2007). The MAPK(ERK-1,2) pathway integrates distinct and antagonistic signals from TGFalpha and FGF7 in morphogenesis of mouse mammary epithelium. Dev. Biol. *306*, 193–207.

Godde, N.J., Galea, R.C., Elsum, I.A., and Humbert, P.O. (2010). Cell polarity in motion: redefining mammary tissue organization through EMT and cell polarity transitions. J. Mammary Gland Biol. Neoplasia *15*, 149–168.

Gu, B., Sun, P., Yuan, Y., Moraes, R.C., Li, A., Teng, A., Agrawal, A., Rhéaume, C., Bilanchone, V., Veltmaat, J.M., et al. (2009). Pygo2 expands mammary progenitor cells by facilitating histone H3 K4 methylation. J. Cell Biol. *185*, 811–826.

Gu, B., Watanabe, K., Sun, P., Fallahi, M., and Dai, X. (2013). Chromatin effector Pygo2 mediates Wnt-notch crosstalk to suppress luminal/alveolar potential of mammary stem and basal cells. Cell Stem Cell *13*, 48–61.

Guo, W., Keckesova, Z., Donaher, J.L., Shibue, T., Tischler, V., Reinhardt, F., Itzkovitz, S., Noske, A., Zürrer-Härdi, U., Bell, G., et al. (2012). Slug and Sox9 cooperatively determine the mammary stem cell state. Cell *148*, 1015–1028.

Hoeflich, K.P., O'Brien, C., Boyd, Z., Cavet, G., Guerrero, S., Jung, K., Januario, T., Savage, H., Punnoose, E., Truong, T., et al. (2009). In vivo antitumor activity of MEK and phosphatidylinositol 3-kinase inhibitors in basal-like breast cancer models. Clin. Cancer Res. *15*, 4649–4664.

Kalluri, R., and Weinberg, R.A. (2009). The basics of epithelial-mesenchymal transition. J. Clin. Invest. *119*, 1420–1428.

Kouros-Mehr, H., and Werb, Z. (2006). Candidate regulators of mammary branching morphogenesis identified by genome-wide transcript analysis. Dev. Dyn. *235*, 3404–3412.

Kurima, K., Hertzano, R., Gavrilova, O., Monahan, K., Shpargel, K.B., Nadaraja, G., Kawashima, Y., Lee, K.Y., Ito, T., Higashi, Y., et al. (2011). A noncoding point mutation of Zeb1 causes multiple developmental malformations and obesity in Twirler mice. PLoS Genet. *7*, e1002307.

Lee, B., Villarreal-Ponce, A., Fallahi, M., Ovadia, J., Sun, P., Yu, Q.-C., Ito, S., Sinha, S., Nie, Q., and Dai, X. (2014). Transcriptional mechanisms link epithelial plasticity to adhesion and differentiation of epidermal progenitor cells. Dev. Cell *29*, this issue, 47–58.

Li, B., Dai, Q., Li, L., Nair, M., Mackay, D.R., and Dai, X. (2002). Ovol2, a mammalian homolog of Drosophila ovo: gene structure, chromosomal mapping, and aberrant expression in blind-sterile mice. Genomics *80*, 319–325.

Li, B., Nair, M., Mackay, D.R., Bilanchone, V., Hu, M., Fallahi, M., Song, H., Dai, Q., Cohen, P.E., and Dai, X. (2005). Ovol1 regulates meiotic pachytene progression during spermatogenesis by repressing Id2 expression. Development *132*, 1463–1473.

Li, R., Liang, J., Ni, S., Zhou, T., Qing, X., Li, H., He, W., Chen, J., Li, F., Zhuang, Q., Qin, B., et al. (2010). A mesenchymal-to-epithelial transition initiates and is required for the nuclear reprogramming of mouse fibroblasts. Cell Stem Cell *7*, 51–63.

Mailleux, A.A., Overholtzer, M., and Brugge, J.S. (2008). Lumen formation during mammary epithelial morphogenesis: insights from in vitro and in vivo models. Cell Cycle *7*, 57–62.

Mani, S.A., Guo, W., Liao, M.J., Eaton, E.N., Ayyanan, A., Zhou, A.Y., Brooks, M., Reinhard, F., Zhang, C.C., Shipitsin, M., et al. (2008). The epithelial-mesenchymal transition generates cells with properties of stem cells. Cell *133*, 704–715.

Morris, J.S., Davies, C.R., Griffiths, M.R., Page, M.J., Bruce, J.A., Patel, T., Herath, A., and Gusterson, B.A. (2004). Proteomic analysis of mouse mammary terminal end buds identifies axonal growth cone proteins. Proteomics *4*, 1802–1810.

Moses, H., and Barcellos-Hoff, M.H. (2011). TGF-beta biology in mammary development and breast cancer. Cold Spring Harb. Perspect. Biol. *3*, a003277.

Nair, M., Teng, A., Bilanchone, V., Agrawal, A., Li, B., and Dai, X. (2006). Ovol1 regulates the growth arrest of embryonic epidermal progenitor cells and represses c-myc transcription. J. Cell Biol. *173*, 253–264.

Nair, M., Bilanchone, V., Ortt, K., Sinha, S., and Dai, X. (2007). Ovol1 represses its own transcription by competing with transcription activator c-Myb and by recruiting histone deacetylase activity. Nucleic Acids Res. *35*, 1687–1697.

Nakaya, Y., and Sheng, G. (2013). EMT in developmental morphogenesis. Cancer Lett. *341*, 9–15.

Nanba, D., Nakanishi, Y., and Hieda, Y. (2001). Changes in adhesive properties of epithelial cells during early morphogenesis of the mammary gland. Dev. Growth Differ. *43*, 535–544.

Nassour, M., Idoux-Gillet, Y., Selmi, A., Côme, C., Faraldo, M.L., Deugnier, M.A., and Savagner, P. (2012). Slug controls stem/progenitor cell growth dynamics during mammary gland morphogenesis. PLoS ONE *7*, e53498.

Nguyen-Ngoc, K.V., Cheung, K.J., Brenot, A., Shamir, E.R., Gray, R.S., Hines, W.C., Yaswen, P., Werb, Z., and Ewald, A.J. (2012). ECM microenvironment regulates collective migration and local dissemination in normal and malignant mammary epithelium. Proc. Natl. Acad. Sci. USA *109*, E2595–E2604.

Piloto, S., and Schilling, T.F. (2010). Ovo1 links Wnt signaling with N-cadherin localization during neural crest migration. Development *137*, 1981–1990.

Rios, A.C., Fu, N.Y., Lindeman, G.J., and Visvader, J.E. (2014). In situ identification of bipotent stem cells in the mammary gland. Nature *506*, 322–327.

Roca, H., Hernandez, J., Weidner, S., McEachin, R.C., Fuller, D., Sud, S., Schumann, T., Wilkinson, J.E., Zaslavsky, A., Li, H., et al. (2013). Transcription factors OVOL1 and OVOL2 induce the mesenchymal to epithelial transition in human cancer. PLoS ONE *8*, e76773.

Roy, S., Gascard, P., Dumont, N., Zhao, J., Pan, D., Petrie, S., Margeta, M., and Tlsty, T.D. (2013). Rare somatic cells from human breast tissue exhibit extensive lineage plasticity. Proc. Natl. Acad. Sci. USA *110*, 4598–4603.

Shackleton, M., Vaillant, F., Simpson, K.J., Stingl, J., Smyth, G.K., Asselin-Labat, M.L., Wu, L., Lindeman, G.J., and Visvader, J.E. (2006). Generation of a functional mammary gland from a single stem cell. Nature *439*, 84–88.

Stingl, J., Eirew, P., Ricketson, I., Shackleton, M., Vaillant, F., Choi, D., Li, H.I., and Eaves, C.J. (2006). Purification and unique properties of mammary epithelial stem cells. Nature *439*, 993–997.

Subramanian, A., Tamayo, P., Mootha, V.K., Mukherjee, S., Ebert, B.L., Gillette, M.A., Paulovich, A., Pomeroy, S.L., Golub, T.R., Lander, E.S., and Mesirov, J.P. (2005). Gene set enrichment analysis: a knowledge-based approach for interpreting genome-wide expression profiles. Proc. Natl. Acad. Sci. USA *102*, 15545–15550.

Takahashi, K., and Yamanaka, S. (2006). Induction of pluripotent stem cells from mouse embryonic and adult fibroblast cultures by defined factors. Cell *126*, 663–676.

Thiery, J.P., Acloque, H., Huang, R.Y., and Nieto, M.A. (2009). Epithelial-mesenchymal transitions in development and disease. Cell *139*, 871–890.

Tsukamoto, A.S., Grosschedl, R., Guzman, R.C., Parslow, T., and Varmus, H.E. (1988). Expression of the int-1 gene in transgenic mice is associated with mammary gland hyperplasia and adenocarcinomas in male and female mice. Cell *55*, 619–625.

Unezaki, S., Horai, R., Sudo, K., Iwakura, Y., and Ito, S. (2007). Ovol2/Movo, a homologue of Drosophila ovo, is required for angiogenesis, heart formation and placental development in mice. Genes Cells *12*, 773–785.

Valastyan, S., and Weinberg, R.A. (2011). Tumor metastasis: molecular insights and evolving paradigms. Cell *147*, 275–292.

Van Keymeulen, A., Rocha, A.S., Ousset, M., Beck, B., Bouvencourt, G., Rock, J., Sharma, N., Dekoninck, S., and Blanpain, C. (2011). Distinct stem cells contribute to mammary gland development and maintenance. Nature *479*, 189–193.

Watanabe, K., Fallahi, M., and Dai, X. (2014). Chromatin effector Pygo2 regulates mammary tumor initiation and heterogeneity in MMTV-Wnt1 mice. Oncogene. *33*, 632–642.

Watson, C.J., and Khaled, W.T. (2008). Mammary development in the embryo and adult: a journey of morphogenesis and commitment. Development *135*, 995–1003.

Wells, J., Lee, B., Cai, A.Q., Karapetyan, A., Lee, W.J., Rugg, E., Sinha, S., Nie, Q., and Dai, X. (2009). Ovol2 suppresses cell cycling and terminal differentiation of keratinocytes by directly repressing c-Myc and Notch1. J. Biol. Chem. *284*, 29125–29135.

Welm, B.E., Dijkgraaf, G.J., Bledau, A.S., Welm, A.L., and Werb, Z. (2008). Lentiviral transduction of mammary stem cells for analysis of gene function during development and cancer. Cell Stem Cell *2*, 90–102.

Williams, C., Helguero, L., Edvardsson, K., Haldosén, L.A., and Gustafsson, J.A. (2009). Gene expression in murine mammary epithelial stem cell-like cells shows similarities to human breast cancer gene expression. Breast Cancer Res. *11*, R26.

Xu, J., Lamouille, S., and Derynck, R. (2009). TGF-beta-induced epithelial to mesenchymal transition. Cell Res. *19*, 156–172.

Zhang, T., Zhu, Q., Xie, Z., Chen, Y., Qiao, Y., Li, L., and Jing, N. (2013). The zinc finger transcription factor Ovol2 acts downstream of the bone morphogenetic protein pathway to regulate the cell fate decision between neuroectoderm and mesendoderm. J. Biol. Chem. *288*, 6166–6177.